Applied Mathematics. 2011; 1(2): 90-98
DOI: 10.5923/j.am.20110102.15

Conjugate Transient Free Convective Heat Transfer from a Vertical Slender Hollow Cylinder with Heat Generation Effect

H. P. Rani*, G Janardhana Reddy

Department of Mathematics, National Institute of Technology, Warangal, 506004, India

Abstract Numerical analysis is performed to study the conjugate heat transfer and heat generation effects on the transient free convective boundary layer flow over a vertical slender hollow circular cylinder with the inner surface at a constant temperature. A set of non-dimensional governing equations namely, the continuity, momentum and energy equations is derived and these equations are unsteady non-linear and coupled. As there is no analytical or direct numerical method available to solve these equations, they are solved using the CFD techniques. An unconditionally stable Crank-Nicolson type of implicit finite difference scheme is employed to obtain the discretized forms of the governing equations. The discretized equations are solved using the tridiagonal algorithm. Numerical results for the transient velocity and temperature profiles, average skin-friction coefficient and average Nusselt number are shown graphically. In all these profiles it is observed that the time required to reach the steady-state increases as the conjugate-conduction parameter or heat generation parameter increases.

Keywords Conjugate Heat Transfer, Heat Generation, Natural Convection, Vertical Slender Hollow Cylinder, Finite Difference Method

1. Introduction

Transient natural convection flow of a viscous incompressible fluid with heat transfer is an important problem relevant to many engineering applications. They have wide applications in Science and Technology. These types of problems are commonly encountered in start-up of a chemical reactor and emergency cooling of a nuclear fuel element. In the case of power or pump failure, similar conditions may arise for devices cooled by forced circulation, as in the core of a nuclear reactor. In the glass and polymer industries, hot filaments, which are considered as a vertical cylinder, are cooled as they pass through the surrounding environment. The exact solution for these types of non-linear problems is still out of reach. Sparrow and Gregg[1] provided the first approximate solution for the laminar buoyant flow of air bathing a vertical cylinder heated with a prescribed surface temperature, by applying the similarity method and power series expansion. Minkowycz and Sparrow[2] obtained the solution for the same problem using the non-similarity method. While Fujii and Uehara[3] analyzed the local heat transfer results for arbitrary Prandtl numbers. Lee et al.[4] investigated the similar problem along slender vertical cylinders and needles for the power-law variation in the wall temperature. In general, Bottemanne 5] studied the combined effect of heat and mass transfer in the steady laminar boundary layer of a vertical cylinder for air and water vapour. Recently, Rani and Kim 6] investigated the unsteady effects for the similar problem with temperature dependent viscosity.

It can be observed that in the previous investigations the wall conduction resistance in the case of convective heat transfer between a solid cylinder wall and a fluid flow is generally neglected i.e. the wall is assumed to be very thin and there is no conduction from the cylinder wall. But in many practical problems the information on the interfacial temperature is essential because the heat transfer characteristics are mainly determined by the temperature differences between the bulk flow and the interface. In order to take account of physical reality, there has been a proclivity to move away from considering idealized mathematical problems in which the bounding wall is considered to be infinitesimally thin. Thus the conduction in solid wall and the convection in the fluid should be determined simultaneously. This type of convective heat transfer is referred to as a conjugate heat transfer (CHT) process and it arises due to the finite thickness of the wall. These type of problems are usually referred to as conjugate heat transfer problems, and they have many practical applications, particularly those related

* Corresponding author:
hprani@nitw.ac.in (H. P. Rani)
Published online at http://journal.sapub.org/am

to energy conservation in buildings, cold storage installations and cryogenic applications, such as medical and space technology. The early theoretical and experimental work of CHT problem for a viscous fluid has been reviewed by Gdalevich and Fertman[7] and Miyamoto et al.[8]. Gdalevich and Fertman[7] gave review about the conjugate problems of free convection with the details about the methods, specifics and principal results. They stated conclusively that the use of numerical methods for solving the initial system of governing partial differential equations, such as finite difference method, is evidently the most promising in the studies of conjugate free convection. Char et al.[9] employed the cubic spline collocation numerical method to analyze the CHT in the laminar boundary layer on a continuous, moving plate. Pop et al.[10] presented a detailed numerical study of the conjugate mixed convection flow along a vertical flat plate. Pop and Na[11] reported a numerical study of the steady conjugate free convection over a vertical slender, hollow circular cylinder with the inner surface at a constant temperature and embedded in a porous medium. Recently, Kaya[12] studied the effects of buoyancy and CHT on non-Darcy mixed convection about a vertical slender hollow cylinder embedded in a porous medium with high porosity.

The CHT problems associated with the heat generating plate were studied by Karvinen[13], Sparrow et al.[14] and Garg et al.[15] using an approximate method. Analytical and numerical solutions were performed by Vynnycky et al.[16] for the CHT problem associated with the forced convection flow over a conducting slab sited in an aligned uniform stream. Vajravelu and Hadjinicolaou[17] analyzed the heat transfer behavior within the boundary layer of a viscous fluid over a stretching sheet with viscous dissipation and internal heat generation. Moreover, effects of heat generation/absorption and thermophoresis on hydromagnetic flow along a flat plate were studied by Chamkha and Camille[18]. Recently, Mamun et al.[19] investigated the effects of magnetic field, viscous dissipation and heat generation on natural convection flow along and conduction inside a vertical flat plate.

From the above studies, it can be noted that the CHT on the unsteady natural convective flow of a viscous incompressible fluid over a vertical cylinder with heat generation has received very scant attention in the literature. Hence, in the present investigation our attention is focused on the effect of heat generation on the coupling of conduction inside and the laminar natural convection flow over the outside surface of a vertical slender hollow cylinder. The temperature of the inner surface of the cylinder is kept at a constant value which is higher than the ambient fluid temperature and the temperature of the outer surface is determined by the conjugate solution of the steady-state energy equation of the solid and the boundary layer equations of the fluid flow. The governing equations are solved numerically by the implicit finite difference method to obtain the transient velocity and temperature profiles, coefficient of skin-friction and heat transfer rate for different values of conjugate-conduction and heat generation parameters.

In section 2, a detailed description about the formulation of the problem is given. Also, the governing equations, such as mass, momentum and energy equations of an incompressible fluid flow past a vertical cylinder are derived and non-dimensionalized. In section 3, the details about the grid generation and numerical methods for solving the above governing equations are given. In section 4, transient two-dimensional velocity and temperature profiles, average skin-friction coefficient and heat transfer rate are analyzed. Finally, the concluding remarks are made in section 5.

2. Mathematical Formulation

An unsteady two-dimensional laminar natural convection boundary layer flow of a viscous incompressible fluid past a vertical slender hollow cylinder of length l and outer radius r_0 ($l >> r_0$) is considered as shown in Fig. 1. The x-axis is measured vertically upward along the axis of the cylinder. The origin of x is taken to be at the leading edge of the cylinder, where the boundary layer thickness is zero. The radial coordinate, r, is measured perpendicular to the axis of the cylinder. The surrounding stationary fluid temperature is assumed to be of ambient temperature (T'_∞). The temperature of the inside surface of the cylinder is maintained at a constant temperature of T_0', where $T_0' > T_\infty'$. Initially, i.e., at time $t' = 0$ it is assumed that the outer surface of the cylinder and the fluid are of the same temperature T'_∞. As time increases ($t' > 0$), the temperature of the outer surface of the cylinder is raised to the solid-fluid interface temperature T_w' and maintained at the same level for all time $t' > 0$. This temperature T_w' is determined by the conjugate solution of the steady-state energy equation of the solid and the boundary layer equations of the fluid flow and is discussed elsewhere. It is assumed that the effect of viscous dissipation is negligible in the energy equation. Under these assumptions, the boundary layer equations of mass, momentum and energy with Boussinesq's approximation are as follows:

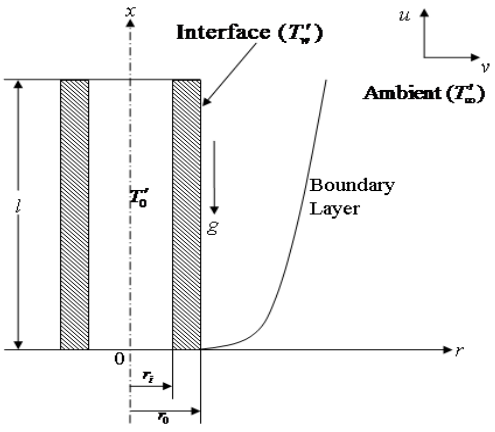

Figure 1. Schematic of the investigated problem

$$\frac{\partial (ru)}{\partial x} + \frac{\partial (rv)}{\partial r} = 0 \tag{1}$$

$$\rho\left(\frac{\partial u}{\partial t'}+u\frac{\partial u}{\partial x}+v\frac{\partial u}{\partial r}\right)=\rho g\beta(T'-T_\infty')+\frac{1}{r}\frac{\partial}{\partial r}\left(\mu r\frac{\partial u}{\partial r}\right) \quad (2)$$

$$\frac{\partial T'}{\partial t'}+u\frac{\partial T'}{\partial x}+v\frac{\partial T'}{\partial r}=\frac{\alpha}{r}\frac{\partial}{\partial r}\left(r\frac{\partial T'}{\partial r}\right)+\frac{Q_0}{\rho c_p}\left(T'-T_\infty'\right) \quad (3)$$

In the above Eq. (3), the term $\frac{Q_0}{\rho c_p}\left(T'-T_\infty'\right)$, Q_0 being a constant, represents the amount of generated or absorbed heat per unit volume. Heat is generated or absorbed from the source term according as Q_0 is positive or negative.

The corresponding initial and boundary conditions are given by

$$\begin{aligned} t'\le 0 &: u=0,\ v=0,\ T'=T_\infty' \quad \text{for all } x \text{ and } r \\ t'>0 &: u=0,\ v=0,\ T'=T_w' \quad \text{at } r=r_0 \\ &\quad u=0,\ v=0,\ T'=T_\infty' \quad \text{at } x=0 \\ &\quad u\to 0,\ v\to 0,\ T'\to T_\infty' \quad \text{as } r\to\infty \end{aligned} \quad (4)$$

where T_w' is the unknown solid-fluid interface temperature and is determined as follows:

To predict the outer surface temperature of the cylinder T_w', an additional governing equation is required for the slender hollow cylinder based on the simplification that the wall of cylinder steady transfers its heat to the surrounding fluid. Since the outer radius of the hollow cylinder, r_0, is small compared to its length, *l*, the axial conduction term in the heat conduction equation of the cylinder can be omitted. The governing equation for the temperature distribution within the slender hollow circular cylinder is given by Chang 20] as follows:

$$\frac{\partial^2 T_s'}{\partial r^2}+\frac{1}{r}\frac{\partial T_s'}{\partial r}=0;\quad 0\le x\le l;\ r_i\le r\le r_0 \quad (5)$$

subject to

$$\begin{aligned} T_s'&=T_0' \text{ at } r=r_i \\ T_s'&=T_w'=T'(x,r_0) \text{ at } r=r_0 \end{aligned} \quad (6)$$

The general solution of Eq. (5) along with (6) is given by

$$T_s'=T_0'+(T'(x,r_0)-T_0')\frac{\ln(r/r_i)}{\ln(r_0/r_i)} \quad (7)$$

On the other hand, Eq. (5) is coupled with the energy equation in the fluid region based on the condition that the temperature and the heat flux are continuous at the solid-fluid interface, namely

$$T_s'=T'(x,r_0),\ -k_s\frac{\partial T_s'}{\partial r}=-k_f\frac{\partial T'(x,r_0)}{\partial r} \text{ on } r=r_0 \quad (8)$$

Using Eqs. (7) and (8), the temperature distribution T_w' at the interface is given by

$$T_w'=T'(x,r_0)=r_0\frac{k_f}{k_s}\ln\left(\frac{r_0}{r_i}\right)\frac{\partial T'(x,r_0)}{\partial r}+T_0' \text{ at } r=r_0 \quad (9)$$

By introducing the following non-dimensional quantities

$$X=Gr^{-1}\frac{x}{r_0},\ R=\frac{r}{r_0},\ U=Gr^{-1}\frac{u\,r_0}{\upsilon},\ V=\frac{v\,r_0}{\upsilon},\ t=\frac{\upsilon\,t'}{r_0^2},$$

$$T=\frac{T'-T_\infty'}{T_0'-T_\infty'},\ Gr=\frac{g\,\beta\,r_0^3(T_0'-T_\infty')}{\upsilon^2},\ Pr=\frac{\upsilon}{\alpha},$$

$$Q=\frac{Q_0 r_0^2}{c_p\mu},\ P=\frac{k_f}{k_s}\ln\left(\frac{r_0}{r_i}\right) \quad (10)$$

(the symbols are explained in the nomenclature) in the Eqs. (1)-(3), they reduced to the following form:

$$\frac{\partial U}{\partial X}+\frac{\partial V}{\partial R}+\frac{V}{R}=0 \quad (11)$$

$$\frac{\partial U}{\partial t}+U\frac{\partial U}{\partial X}+V\frac{\partial U}{\partial R}=T+\left(\frac{\partial^2 U}{\partial R^2}+\frac{1}{R}\frac{\partial U}{\partial R}\right) \quad (12)$$

$$\frac{\partial T}{\partial t}+U\frac{\partial T}{\partial X}+V\frac{\partial T}{\partial R}=\frac{1}{Pr}\left(\frac{\partial^2 T}{\partial R^2}+\frac{1}{R}\frac{\partial T}{\partial R}\right)+QT \quad (13)$$

The corresponding initial and boundary conditions in non-dimensional quantities are given by

$$\begin{aligned} t\le 0 &: U=0,\ V=0,\ T=0 \quad \text{for all } X \text{ and } R \\ t>0 &: U=0,\ V=0,\ T-1=P\frac{\partial T}{\partial R} \quad \text{at } R=1 \\ &\quad U=0,\ V=0,\ T=0 \quad \text{at } X=0 \\ &\quad U\to 0,\ V\to 0,\ T\to 0 \quad \text{as } R\to\infty \end{aligned} \quad (14)$$

3. Numerical Solution

In order to solve the unsteady coupled non-linear governing Eqs. (11)-(13) an implicit finite difference scheme of Crank-Nicolson type has been employed. The finite difference equations corresponding to Eqs. (11) - (13) are as follows:

$$\frac{U_{i,j}^{k+1}-U_{i-1,j}^{k+1}+U_{i,j}^{k}-U_{i-1,j}^{k}}{\Delta X}+\frac{V_{i,j+1}^{k+1}-V_{i,j-1}^{k+1}+V_{i,j+1}^{k}-V_{i,j-1}^{k}}{2\,\Delta R}+\frac{V_{i,j}^{k+1}+V_{i,j}^{k}}{\left[1+(j-1)\Delta R\right]}=0 \quad (15)$$

$$\frac{U_{i,j}^{k+1}-U_{i,j}^{k}}{\Delta t}+\frac{U_{i,j}^{k}}{2\,\Delta X}(U_{i,j}^{k+1}-U_{i-1,j}^{k+1}+U_{i,j}^{k}-U_{i-1,j}^{k})+\frac{V_{i,j}^{k}}{4\,\Delta R}(U_{i,j+1}^{k+1}-U_{i,j-1}^{k+1}+U_{i,j+1}^{k}-U_{i,j-1}^{k})=\frac{T_{i,j}^{k+1}+T_{i,j}^{k}}{2}+\left(\frac{U_{i,j+1}^{k+1}-U_{i,j-1}^{k+1}+U_{i,j+1}^{k}-U_{i,j-1}^{k}}{4\left[1+(j-1)\Delta R\right]\Delta R}\right)+\left(\frac{U_{i,j-1}^{k+1}-2U_{i,j}^{k+1}+U_{i,j+1}^{k+1}+U_{i,j-1}^{k}-2U_{i,j}^{k}+U_{i,j+1}^{k}}{2(\Delta R)^2}\right) \quad (16)$$

$$\frac{T_{i,j}^{k+1}-T_{i,j}^{k}}{\Delta t}+\frac{U_{i,j}^{k}}{2\Delta X}(T_{i,j}^{k+1}-T_{i-1,j}^{k+1}+T_{i,j}^{k}-T_{i-1,j}^{k})+\frac{V_{i,j}^{k}}{4\Delta R}(T_{i,j+1}^{k+1}-T_{i,j-1}^{k+1}+T_{i,j+1}^{k}-T_{i,j-1}^{k})$$

$$= \left(\frac{T_{i,j-1}^{k+1} - 2T_{i,j}^{k+1} + T_{i,j+1}^{k+1} + T_{i,j-1}^{k} - 2T_{i,j}^{k} + T_{i,j+1}^{k}}{2Pr(\Delta R)^2} \right)$$

$$+ \left(\frac{T_{i,j+1}^{k+1} - T_{i,j-1}^{k+1} + T_{i,j+1}^{k} - T_{i,j-1}^{k}}{4Pr\left[1+(j-1)\Delta R\right]\Delta R} \right) + Q\left(\frac{T_{i,j}^{k+1} + T_{i,j}^{k}}{2} \right) \quad (17)$$

To solve the finite difference Eqs. (15)-(17), the region of integration is considered as a rectangle composed of the lines indicating $X_{\min} = 0$, $X_{\max} = 1$, $R_{\min} = 1$ and $R_{\max} = 16$, where $R_{\max}$ corresponds to $R = \infty$ which lies very far from the momentum and energy boundary layers. In the above Eqs. (15)-(17) the subscripts i and j designate the grid points along the X and R coordinates, respectively, where $X = i\,\Delta X$ and $R = 1 + (j - 1)\,\Delta R$ and the superscript k designates a value of the time t ($= k\,\Delta t$), with ΔX, ΔR and Δt the mesh size in the X, R and t axes, respectively. In order to obtain an economical and reliable grid system for the computations, a grid independent test has been performed which is shown in Fig. 2. The steady-state velocity and temperature values obtained with the grid system of 100 × 500 differ in the second decimal place from those with the grid system of 50 × 250, and in the fifth decimal place from those with the grid system of 200 × 1000. Hence, the grid system of 100 × 500 has been selected for all subsequent analyses, with mesh size in X and R direction are taken as 0.01 and 0.03, respectively. Also, the time step size dependency has been carried out, from which 0.01 yielded a reliable result.

From the initial conditions given in Eq. (14), the values of velocity U, V and temperature T are known at time $t = 0$, then the values of T, U and V at the next time step can be calculated. Generally, when the above variables are known at $t = k\,\Delta t$, the variables at $t = (k + 1)\,\Delta t$ are calculated as follows. The finite difference Eqs. (16) and (17) at every internal nodal point on a particular i-level constitute a tridiagonal system of equations. Such a system of equations is solved by the Thomas algorithm (Carnahan et al. 21]). At first, the temperature T is calculated from Eq. (17) at every j nodal point on a particular i-level at the $(k + 1)$th time step. By making use of these known values of T, the velocity U at the $(k+1)$th time step is calculated from Eq. (16) in a similar manner. Thus, the values of T and U are known at a particular i-level. Then the velocity V is calculated from Eq. (15) explicitly. This process is repeated for the consecutive i-levels; thus the values of T, U and V are known at all grid points in the rectangular region at the $(k + 1)$th time step. This iterative procedure is repeated for many time steps until the steady-state solution is reached. The steady-state solution is assumed to have been reached when the absolute difference between the values of velocity as well as temperature at two consecutive time steps is less than 10^{-5} at all grid points. The truncation error in the employed finite difference approximation is $O(\Delta t^2 + \Delta R^2 + \Delta X)$ and tends to zero as ΔX, ΔR and $\Delta t \to 0$. Hence the system is compatible. Also, this finite difference scheme is unconditionally stable and therefore, stability and compatibility ensure convergence.

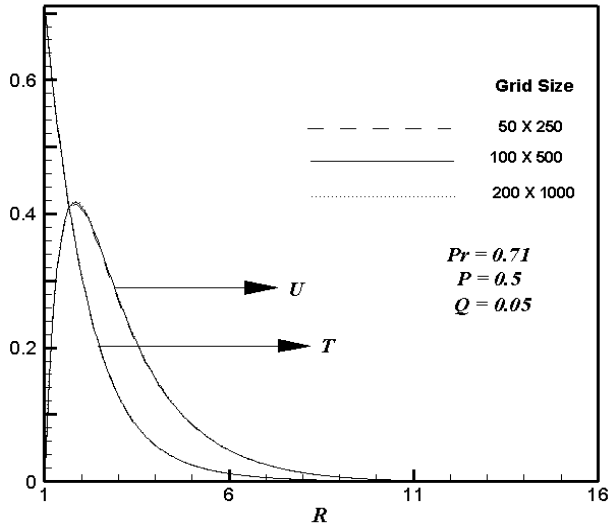

Figure 2. Grid independent test for velocity and temperature profiles

4. Results and Discussion

To validate the current numerical procedure, the present simulated velocity and temperature profiles are compared with those of the available steady-state, isothermal results of Lee et al. 4] for air (Pr = 0.7) without conduction and heat generating effects i.e., P = 0.0 and Q = 0.0, as there are no experimental or analytical studies available to compare with the present problem. The current results are found to be in good agreement with the previous results available in literature as shown in Fig. 3.

The simulated results are presented to outline the general physics involved in the effects of different Q (= 0.01, 0.05, 0.08 and 0.10) 19] and P (= 0.1, 0.5, 1.0 and 2.0) 11] with fixed Pr [= 0.71 (air)] on the transient velocity and temperature profiles. The simulated transient behaviour of the dimensionless velocity, temperature, average skin-friction coefficient and heat transfer rate are discussed in detail in the succeeding subsections.

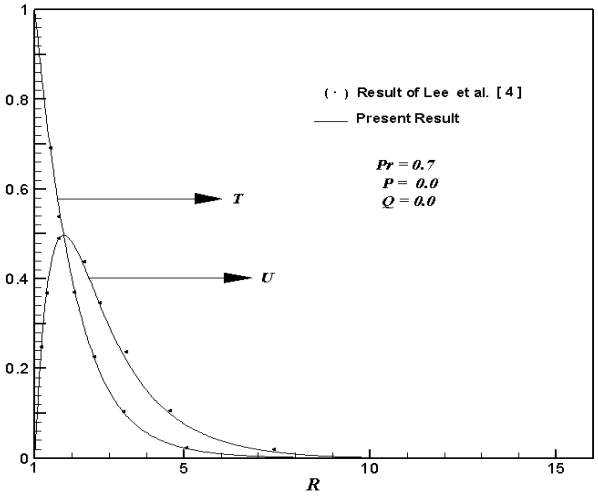

Figure 3. Comparison of the velocity and temperature profiles

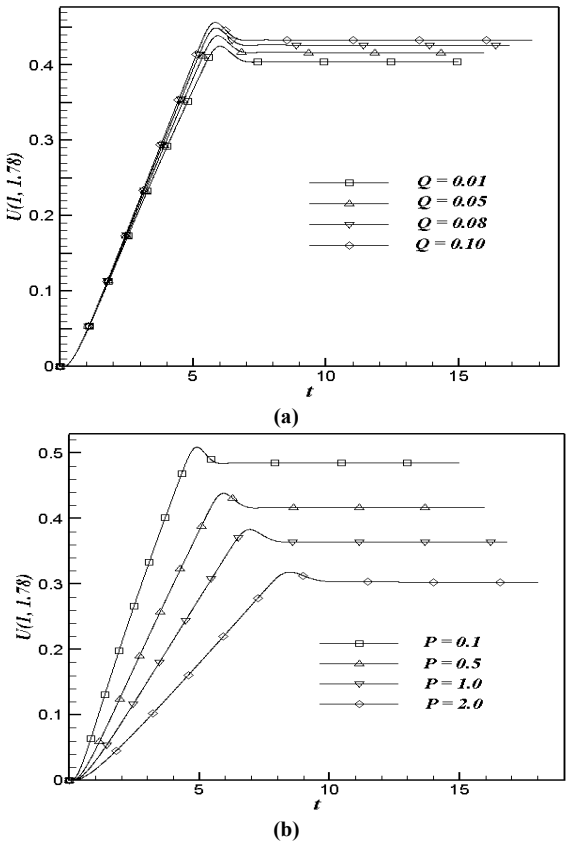

Figure 4. The simulated transient velocity at (1, 1.78) for (a) variation of Q with fixed $P = 0.5$; (b) variation of P with fixed $Q = 0.05$

4.1. Velocity

The simulated transient velocity (U) at (1, 1.78) for different values of heat generation parameter Q and conjugate-conduction parameter P against t is shown graphically in Fig. 4. Fig. 4a shows the variation of Q with fixed $P = 0.5$ and Fig. 4b for the variation of P with fixed $Q = 0.05$. From Figs. 4a and 4b it is observed that the velocity increases with time, reaches a temporal maximum, then decreases and at last reaches the asymptotic steady-state. For example, in Fig. 4a when $Q = 0.01$, the velocity increases with time monotonically from zero and reaches the temporal maximum, then slightly decreases with time and becomes asymptotically steady. It is observed that at the very early time (i.e., $t << 1$), the heat transfer is dominated by conduction. Shortly later, there exists a period when the heat transfer rate is influenced by the effect of convection with the increasing upward velocities along the time. When this transient period is almost ending and just before the steady-state is about to be reached, there exist overshoots of the velocities. From Figs. 5a and 5b it can be observed that velocity profiles reach their maximum value approximately at (1, 1.78). Similarly, the velocity at other locations also exhibits somewhat similar transient behaviour. As noted in Fig. 4a, the magnitude of this overshoot of the velocities increases as Q is increased, since with the increasing Q the velocity diffusion is decreased (refer Eq. (12)). Hence, there is a high resistance to the fluid flow in the region of the temporal maximum of velocity. The time needed to reach the temporal maximum of the velocity increases as Q increases. It is also noticed that for small values of Q the temporal maximum is reached at early times. For all values of P, Figure 4b reveals that it has the same trend as the transient behaviour with respect to Q shown in Fig. 4a, but the temporal maximum of velocity decreases as P increases. In association with the transient characteristics of the velocity, similar trends of the temperature fluctuation can be observed and will be described in Fig. 6.

Figure 5 shows the simulated steady-state velocity profiles against the R at $X = 1.0$ for different values of Q and P. Fig. 5a shows the variation of Q with fixed $P = 0.5$ and Fig. 5b for the variation of P with fixed $Q = 0.05$. From these figures it is observed that the velocity profile start with the value zero at the wall, reach their maximum and then monotonically decrease to zero along the radial coordinate for all t. Also it is observed that in the vicinity of the wall the magnitude of the axial velocity is rapidly increasing as R increases from R_{min} (=1). From Fig. 5a it is observed that the velocity increases with the increasing values of Q because the effect of velocity diffusion gets decreased for high values of Q. When Q is increased, the thermal convection is confined to a region near the hot wall, while the momentum diffusion is propagated far from the hot wall and hence the high velocity profiles are observed close to the hot wall. It is also observed that the time required to reach the steady-state increases as Q increases. Fig. 5b reveals that it has the same trend as the variation of steady-state time with respect to Q as shown in Fig. 5a, but the velocity profile is influenced significantly and decreases when the value of P increases.

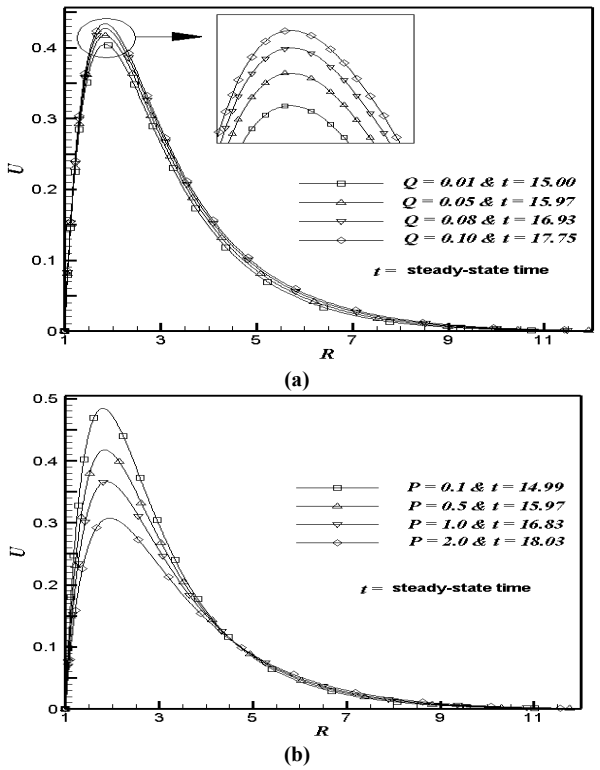

Figure 5. The simulated steady-state velocity profile at $X = 1.0$ for (a) variation of Q with fixed $P = 0.5$; (b) variation of P with fixed $Q = 0.05$

4.2. Temperature

The simulated transient temperature (T) for different values of Q and P with respect to t is shown at the point (1, 1.09)

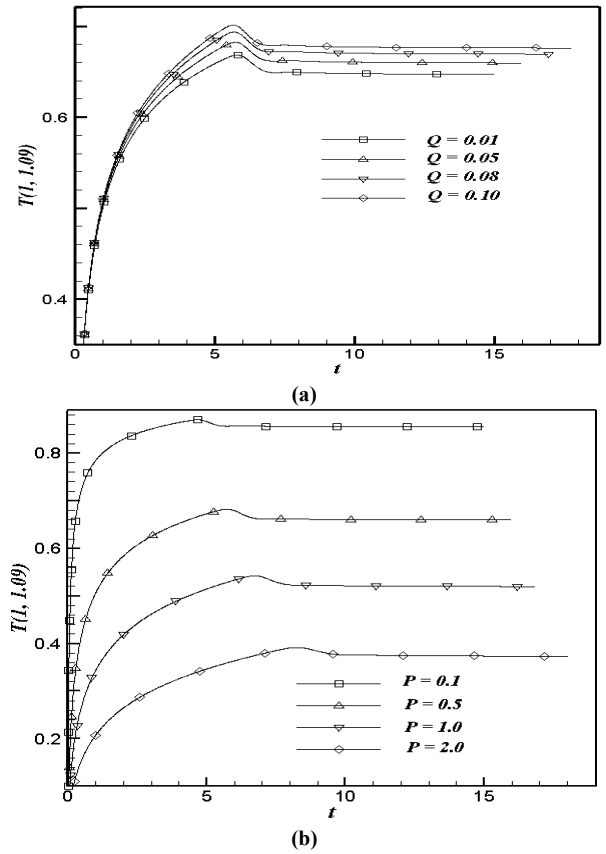

Figure 6. The simulated transient temperature at (1, 1.09) for (a) variation of Q with fixed P = 0.5; (b) variation of P with fixed Q = 0.05

in Fig. 6. Figure 6a shows the variation of Q with fixed P = 0.5 and Fig. 6b for the variation of P with fixed Q = 0.05. From Figs. 6a and 6b it is observed that these profiles increase with time, reach a temporal maximum, decrease and again after a slight increase attain the steady-state asymptotically. The temperature at other locations also exhibits somewhat similar transient behaviour. During the initial period, the nature of the transient temperature profiles is particularly noticeable. From Fig. 6a it is observed that for all values of Q, the transient temperature profiles initially coincide and then deviate after some time. Also, the time required to reach the temporal maximum of the temperature increases with the increasing values of Q. It can be noticed that for small values of Q the temporal maximum is attained at an early times. Here, it is observed that the maximum value of temperature increases with the increasing Q. Figure 6b shows that it has the same trend as the transient behaviour with respect to Q shown in Fig. 6a, but the temporal maximum of temperature decreases as P increases. From Figs. 6a and 6b it is noticed that during the initial time, the variation of temperature with P is observed to be larger than that with Q. This result implies that the temperature field is more strongly affected by the conjugate-conduction parameter, since an increased value of P corresponds to a lower wall conductance k_s and promotes greater surface temperature variations as shown in Fig. 6b.

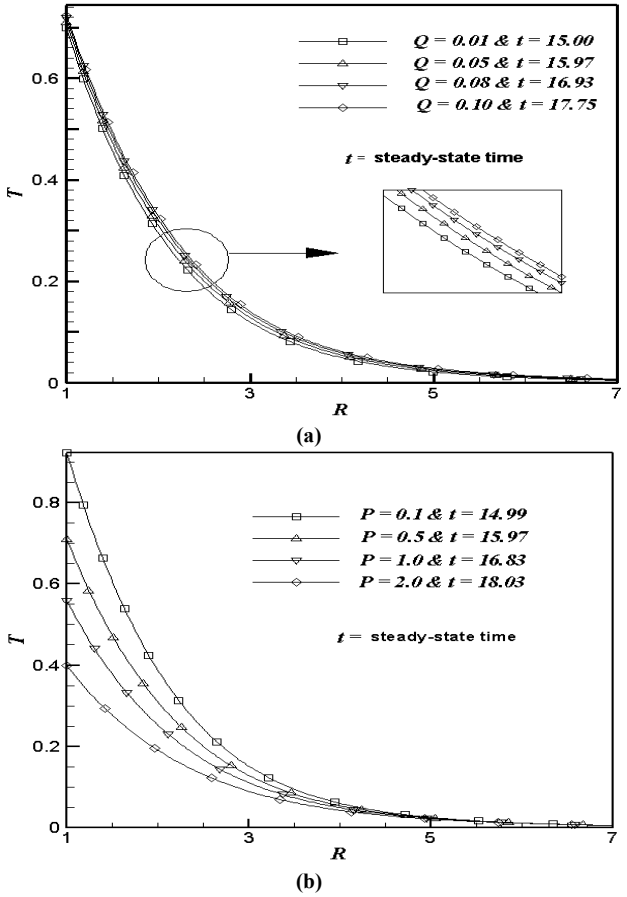

Figure 7. The simulated steady-state temperature profile at X = 1.0 for (a) variation of Q with fixed P = 0.5; (b) variation of P with fixed Q = 0.05

The simulated steady-state temperature profiles for different values of Q and P at X = 1.0 against the R are shown in Fig. 7. Figure 7a depicts the variation of Q with fixed P = 0.5 and Fig. 7b for the variation of P with fixed Q = 0.05. From these figures it is observed that the temperature profiles start with the hot wall temperature and then monotonically decrease to zero along the radial coordinate for all time. It is related to the fact that the effect of velocity diffusion gets increased for higher values of P, which allows higher velocity near the hot wall. From Fig. 7a it is observed that the steady temperature value increases with increasing values of Q for fixed P. Larger Q values give rise to thicker temperature profiles, since a larger Q value means that the thermal diffusion from the wall is prevailing while the velocity diffusion tries to move close to the wall. The increased value of the heat generation parameter means that more heat is produced and eventually, that heat increases the fluid motion as obtained in Figs. 5a and 7a, respectively. Also, time taken to reach the steady-state increases as Q increases. Figure 7b reveals that the steady temperature value decreases as the conduction parameter P increases. A lower wall conductance k_s or higher convective cooling effect due to greater k_f increases the value of P as well as causes greater temperature difference between the two surfaces of the cylinder. This is

due to the reason that the temperature at the solid-fluid interface is reduced since the temperature at the inner surface of the cylinder is kept constant. As a result the temperature profile as well as the velocity profile shifts downwards in the fluid. It is also observed that the time required to reach the steady-state increases as P increases.

4.3. Average Skin-friction Coefficient and Heat Transfer Rate

For engineering purposes, one is usually interested in the values of the skin-friction coefficient and heat transfer rate. The friction coefficient is an important parameter in the heat transfer studies since it is directly related to the heat transfer coefficient. The increased skin-friction is generally a disadvantage in technical applications, while the increased heat transfer can be exploited in some applications such as heat exchangers, but should be avoided in others such as gas turbine applications, for instance. For the present problem these skin-friction coefficient and heat transfer rate are derived and given in the following equations:

The wall shear stress at the wall can be expressed as

$$\tau_w = \left(\mu \frac{\partial u}{\partial r} \right)_{r=r_0} \tag{18}$$

By introducing the non-dimensional quantities given in Eq. (10), the above Eq. (18) can be written as

$$\tau_w = \frac{\mu^2 Gr}{\rho r_0^2} \left(\frac{\partial U}{\partial R} \right)_{R=1} \tag{19}$$

Considering $\frac{\mu^2 Gr}{\rho r_0^2}$ to be the characteristic shear stress, then the local skin-friction coefficient can be written as

$$C_f = \left(\frac{\partial U}{\partial R} \right)_{R=1} \tag{20}$$

The integration of the Eq. (20) from $X = 0$ to $X = 1$ gives the following average skin-friction coefficient.

$$\overline{C_f} = \int_0^1 \left(\frac{\partial U}{\partial R} \right)_{R=1} dX \tag{21}$$

The local Nusselt number is given by

$$Nu_x = \frac{\dot{q}_w r_0}{k_f (T_0' - T_\infty')}, \tag{22}$$

where the heat transfer, $\dot{q}_w$ is given by

$$\dot{q}_w = -k_f \left(\frac{\partial T'}{\partial r} \right)_{r=r_0}$$

Thus, with the non-dimensional quantities introduced in Eq. (10), Eq. (22) can be written as

$$Nu_X = -\left(\frac{\partial T}{\partial R} \right)_{R=1} \tag{23}$$

The integration of the above Eq. (23) with respect to X from 0 to 1 yields the following average Nusselt number.

$$\overline{Nu} = -\int_0^1 \left(\frac{\partial T}{\partial R} \right)_{R=1} dX \tag{24}$$

The derivatives involved in Eqs. (21) and (24) are evaluated by using a five-point approximation formula and then the integrals are evaluated by using the Newton-Cotes closed integration formula. The simulated average non-dimensional skin-friction and heat transfer coefficients have been plotted against the time in Figs. 8 and 9 for different values of Q and P.

The effects of different values of Q and P on the simulated average skin-friction coefficient are shown in Figs. 8a and 8b, respectively. From Figs. 8a and 8b it is observed that for all values of Q and P the average skin-friction coefficient increases with time, attains the peak value and, after slight decrease, reaches asymptotically steady-state. Because the buoyancy-induced flow velocity is relatively low at the initial transient period, as seen in Fig. 4, the wall shear stress remain small, as shown in Fig. 8. However, the wall shear stress increases as the time proceeds, yielding an increase in the skin-friction coefficient. It is also observed from Fig. 8a that for increasing values of Q the average skin-friction coefficient increases. This result lies in the same line with the velocity profiles plotted in Fig 5a. From Fig. 8b it is observed that the average skin-friction coefficient decreases as P increases. It is related to the fact that the increased value of P decreases the velocity of the fluid within the boundary layer, as mentioned in Fig. 5b, and decreases the viscosity of the fluid. It is also noticed that from Figs. 8a and 8b during the initial period, the variation of skin-friction with P is observed to be larger than that with Q. This result means that the average skin-friction coefficient is more strongly affected by P compared to Q.

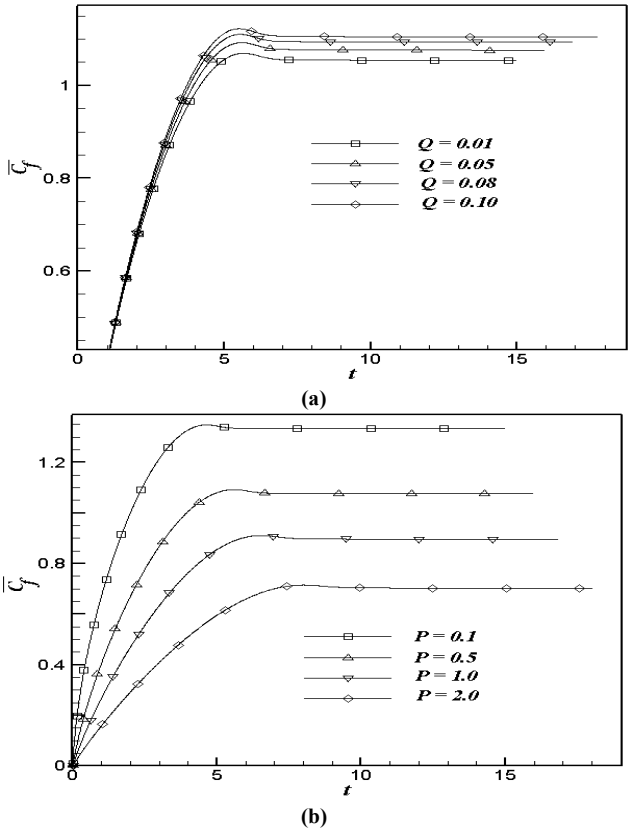

Figure 8. The simulated average skin-friction for (a) variation of Q with fixed $P = 0.5$; (b) variation of P with fixed $Q = 0.05$

In Figs. 9a and 9b the effects of different values of Q and P on the simulated average heat transfer rate are shown, respectively. From Figs. 9a and 9b it is observed that at short times, after $t = 0$, the average Nusselt numbers are almost the same for all values of P and Q. This shows that initially there is only heat conduction. Fig. 9a reveals that an increase in the value of Q leads to a decrease in the values of the average heat transfer rate. Increasing Q retards the spatial decay of the temperature field near the heated surface because of increased flow velocity near the wall, yielding a decrease in the rate of heat transfer. From Fig. 9b it is observed that with the increasing values of P i.e with lower wall conductance (k_s), the average heat transfer rate decreases as P increases.

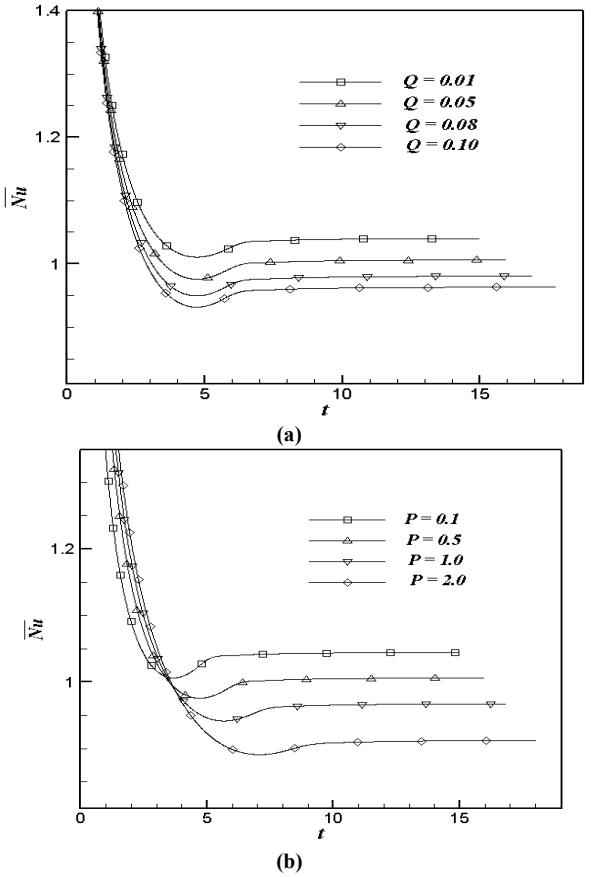

Figure 9. The simulated average Nusselt number for (a) variation of Q with fixed $P = 0.5$; (b) variation of P with fixed $Q = 0.05$

5. Conclusions

A numerical study has been carried out for the conjugate heat transfer on unsteady natural convection boundary layer flow of a viscous incompressible fluid over a vertical slender hollow cylinder with heat generation effect. A Crank-Nicolson type of implicit method is used to solve the governing unsteady, non-linear and coupled equations. The resulting system of equations is solved by using the Thomas algorithm. The computations are carried out for different values of heat generation parameter Q (= 0.01, 0.05, 0.08 and 0.10) and conjugate-conduction parameter P (= 0.1, 0.5, 1.0 and 2.0). For the velocity and temperature profiles it is observed that the time elapsed to reach the temporal maximum increases with the increasing values of Q and P. Time required to reach the steady-state increases as Q or P increases. It is observed that the velocity, temperature and average skin-friction coefficient of the fluid increases with the increasing values of Q. The values of velocity and temperature of the fluid decreases as P increases. It is also noticed that as P or Q increases the steady-state values of average heat transfer rate decreases.

Nomenclature

$\overline{cf}$	dimensionless average skin-friction coefficient
cf	dimensionless local skin-friction coefficient
cp	specific heat at constant pressure
g	acceleration due to gravity
Gr	Grash of number
k_f, k_s	thermal conductivity of the fluid and the solid cylinder, respectively
l	length of the cylinder
$\overline{Nu}$	dimensionless average Nusselt number
Nu_X	dimensionless local Nusselt number
P	conjugate-conduction parameter
Pr	Prandtl number
Q	heat generation parameter
Q_0	constant
r	radial coordinate
r_i, r_0	inner and outer radii of the hollow cylinder,respectively
R	dimensionless radial coordinate
t'	time
t	dimensionless time
T_0'	temperature at the inside surface of the cylinder
T_s'	solid temperature
T'	temperature of the fluid
T	dimensionless temperature of the fluid
u, v	velocity components in x, r directions respectively
U, V	dimensionless velocity components in X, R directions respectively
x	axial coordinate
X	dimensionless axial coordinate

Greek Letters

α	thermal diffusivity
β	volumetric coefficient of thermal expansion
ρ	density
μ	viscosity of the fluid
υ	kinematic viscosity
Subscripts	
w	conditions on the wall
∞	free stream conditions

ACKNOWLEDGEMENTS

The authors wish to acknowledge support for this research work from the Institute Fellowship (National Institute of Technology Warangal).

REFERENCES

[1] Sparrow, E. M., and Gregg, J. L., 1956, Laminar free convection heat transfer from the outer surface of a vertical circular cylinder, ASME Journal of Heat Transfer, 78, 1823-1829.

[2] Minkowycz, W. J., and Sparrow, E. M., 1974, Local nonsimilar solutions for natural convection on a vertical cylinder, ASME Journal of Heat Transfer, 96, 178-183.

[3] Fujii, T., and Uehara, H., 1970, Laminar natural convective heat transfer from the outer surface of a vertical cylinder, International Journal of Heat and Mass Transfer, 13, 607-615.

[4] Lee, H. R., Chen, T. S., and Armaly, B. F., 1988, Natural convection along slender vertical cylinders with variable surface temperature, ASME Journal of Heat Transfer, 110, 103-108.

[5] Bottemanne, F. A., 1972, Experimental results of pure and simultaneous heat and mass transfer by free convection about a vertical cylinder for Pr = 0.71 and Sc = 0.63, Applied Scientific Research, 25, 372-382.

[6] Rani, H. P., and Kim, C. N., 2008, Transient free convection flow over an isothermal vertical cylinder with temperature dependent viscosity, Korean Journal of Chemical Engineering, 25, 34-40.

[7] Gdalevich, L. B., and Fertman, V. E., 1977, Conjugate Problems of Natural Convection, Inzh-Fiz. Zh., 33, 539-547.

[8] Miyamoto, M., Sumikawa, J., Akiyoshi, T., and Nakamura, T., 1980, Effects of Axial Heat Conduction in a Vertical Flat Plate on Free Convection Heat Transfer, International Journal of Heat and Mass Transfer, 23, 1545-1553.

[9] Char, M. I., Chen, C.K., and Cleaver, J. W., 1990, Conjugate forced convection heat transfer from a continuous moving flat sheet, International Journal of Heat and Fluid Flow, 11, 257-261.

[10] Pop, I., Ingham, B., and Yuan, Y., 1996, Mixed convective conjugate heat transfer from a vertical flat plate, ZAMM-Zeitschrift fur Angewandte Mathematik und Mechanik, 76, 281-289.

[11] Pop, I., and Na, T.Y., 2000, Conjugate free convection over a vertical slender hollow cylinder embedded in a porous medium, Heat Mass Transfer, 36, 375-379.

[12] Ahmet Kaya, 2011, Effects of buoyancy and conjugate heat transfer on non-Darcy mixed convection about a vertical slender hollow cylinder embedded in a porous medium with high porosity, International Journal of Heat and Mass Transfer, 54, 818-825.

[13] Karvinen, R., 1978, Some new results for conjugate heat transfer in a flat plate, International Journal of Heat and Mass Transfer, 21, 1261-1264.

[14] Sparrow, E. M., and Chyu, M. K., 1982, Conjugated forced convection-conduction analysis of heat transfer in a plate fin, International Journal of Heat and Mass Transfer, 104, 204–206.

[15] Garg, V. K., and Velusamy, K., 1986, Heat transfer characteristics for a plate fin, Journal of Heat Transfer, 108, 224–226.

[16] Vynnycky, M., Kimura, S., Kanev, K., and Pop, I., 1998, Forced convection heat transfer from a flat plate: the conjugated problem, International Journal of Heat and Mass Transfer, 41, 45–59.

[17] Vajravelu, K., and Hadjinicolaou, A., 1993, Heat transfer in a viscous fluid over a stretching sheet with viscous dissipation and internal heat generation, International Communications in Heat and Mass Transfer, 20, 417–430.

[18] Chamkha, A. J., and Camille, I., 2000, Effects of heat generation/absorption and the thermophoresis on hydromagnetic flow with heat and mass transfer over a flat plate, International Journal of Numerical Methods and Heat Fluid Flow, 10, 432–448.

[19] Mamun, A. A., Chowdhury, Z. R., Azim, M. A., and Molla, M. M., 2008, MHD-conjugate heat transfer analysis for a vertical flat plate in presence of viscous dissipation and heat generation, International Communications in Heat and Mass Transfer, 35, 1275-1280.

[20] Chang, C. L., 1995, Buoyancy and wall conduction effects on forced convection of micropolar fluid flow along a vertical slender hollow circular cylinder, International Journal of Heat and Mass Transfer, 49, 4932-4942.

[21] B. Carnahan, H. A. Luther and J. O. Wilkes, Applied numerical methods, John Wiley Sons, New York, 1969.